Unraveling the role of the thermal and laser impacts on the blackening of cinnabar in the mural paintings of Pompeii

Silvia Pérez-Diez[1,a] , **Aitor Larrañaga**[2] , **, Juan Manuel Madariaga**[1,3] , **Maite Maguregui**[4,b]

[1] Department of Analytical Chemistry, Faculty of Science and Technology, University of the Basque Country UPV/EHU, P.O. Box 644, 48080 Bilbao, Basque Country, Spain
[2] General Research Services (SGIKer), University of the Basque Country UPV/EHU, P.O. Box 644, 48080 Bilbao, Basque Country, Spain
[3] Unesco Chair on Cultural Landscape and Heritage, University of the Basque Country UPV/EHU, 01008 Vitoria-Gasteiz, Basque Country, Spain
[4] Department of Analytical Chemistry, Faculty of Pharmacy, University of the Basque Country UPV/EHU, P.O. Box 450, 01008 Vitoria-Gasteiz, Basque Country, Spain

Abstract The blackening of red cinnabar (α-HgS) pigment has traditionally been explained by its conversion into black metacinnabar (β-HgS). Scarce is however the scientific evidence that supports this hypothesis in polychrome artworks. As such transition occurs at around 345 °C, the thermal impact of the eruption of Mount Vesuvius in 79 AD could have induced this structural change of the pigment present in the mural paintings of Pompeii. This work aims to assess whether the mentioned volcanic eruption could be responsible of the cinnabar blackening through the formation of metacinnabar. The thermodiffractometry study of cinnabar-decorated fresco mock-ups stated that the formed β-HgS is not stable, observing its reversion into α-HgS. Moreover, sublimation of the cinnabar pictorial layer was registered, also when the cinnabar paint layer was protected by a coating of pyroclastic materials. In real blackened cinnabar Pompeian samples, it was not possible to identify metacinnabar by X-ray diffraction (XRD), but evidence of sublimation of mercury due to the thermal impact was observed. Hence, this blackening seems to be related mainly to the presence of calomel (Hg_2Cl_2) and a gypsum ($CaSO_4 \cdot 2H_2O$) crust as degradation products of red cinnabar and the calcite mortar, respectively, and not to the formation of metacinnabar. Finally, laser-based techniques could also induce modifications in the HgS crystalline structure, resulting in an amorphous black product. Therefore, the elemental and molecular study of the species promoted by laser impact was carried out to avoid false positives in the metacinnabar detection or when the decorated surface has been subjected to laser cleaning.

1 Introduction

Red cinnabar (α-HgS), called $\kappa\iota\nu\nu\acute{\alpha}\beta\alpha\rho\iota$ by Theophrastus of Eresos and *minium* by Pliny the Elder and Vitruvius [1], was one of the most exclusive pigments employed in Roman mural paintings.

Vitruvius and Pliny mentioned that pure cinnabar could be distinguished from lime-adulterated cinnabar [2, 3]. Pure cinnabar would recover its red color after being heated and darkened in an iron plate, whereas an adulterated product would remain black. To obtain the pure cinnabar pigment coming from the homonymous mineral, a purification process was usually conducted to remove the metallic impurities that can affect the final brilliant red color and stability of the pigment. According to Vitruvius, red cinnabar pigment was prepared using mineral brought from Hispania in workshops located between the temples of Flora and Quirino [2]. As Pliny stated [3], the Almadén mines were exploited by the *socii sisaponensis* only when the Emperor considered it pertinent.

In spite of its vivid red color, cinnabar pigment suffers from darkening/blackening [4, 5]. Certain cinnabar decorations from the mural paintings of the Archaeological Park of Pompeii are nowadays almost completely blackened, disrupting the correct hues intended by Roman painters. This is the case of the cinnabar decorations from the southern wall of the Room G in the House of the Golden Cupids (Regio VI 16, 7) [5], where calomel (Hg_2Cl_2) and gypsum ($CaSO_4 \cdot 2H_2O$) were mainly identified.

Consistently to what stated in ancient texts, this blackening has traditionally been attributed to light exposure. The transformation of red trigonal α-HgS into black cubic β-HgS metacinnabar, which is reported to take place at 344 ± 2 °C [6, 7], was assumed at the beginning of the twentieth century and proposed by Eibner and Liberti, among many other authors [8, 9]. More recently, other theories have gained increasing attention, such as the photosensitization of cinnabar induced by chlorides or the reduction of Hg(2) to black Hg(0) [10–13]. Indeed, to the best of our knowledge, the main attributions of metacinnabar as the compound present

[a] e-mail: silvia.perezd@ehu.eus (corresponding author)

[b] e-mail: maite.maguregui@ehu.eus (corresponding author)

in blackened cinnabar were simply accepted in the past based on indirect evidence, since the black hue of metacinnabar perfectly explained the discoloration. In addition, the detection of metacinnabar with conventional portable analytical techniques during in situ studies of cinnabar-decorated artworks has not been straightforward [14]. Nonetheless, in laboratory studies [15], metacinnabar was indeed identified via X-ray diffraction (XRD) in mural paintings and by using pump-probe microscopy in a tempera panel [16].

Ballirano et al. evaluated the possibility of the thermal transformation of cinnabar to metacinnabar in Pompeian wall paintings and its persistence over a time span of two millennia [17]. Whereas the maximum estimated temperature of a pyroclastic deposit in Pompeii has been established by Cioni et al. at around 380 °C (being most of the data in the 240–340 °C range) [18], Ballirano et al. stated that the transition needed a higher temperature (425 °C) to take place in an oxidizing atmosphere. The kinetics of the metacinnabar into cinnabar reversion was assessed by XRD: In 4 months, only 45% of the conversion had already occurred, whereas a 99% conversion was calculated to be completed in 8 years. The authors also studied the supposedly light-induced cinnabar into metacinnabar transition, which was probably due to the overheating of the samples and not the light itself [17].

A series of studies have also concerned the blackening of cinnabar induced by Q-switched Nd:YAG lasers (1064 nm), widely employed for cleaning purposes in conservation and restoration treatments. Attention has been devoted to darkening provoked by Raman lasers as well or, more recently, to pump-probe microscopy femtoseconds lasers [16, 19].

Pouli et al. attributed this last darkening to the presence of Hg(0) or Hg(2) (Hg$_2$S) via XPS measurements on laser-irradiated surfaces (Q-switched Nd:YAG) [20], whereas Zafiropulos et al. reported the formation of metacinnabar (15% conversion) due to the thermal effects associated with the laser irradiation [21]. The same authors also pointed out that the presence of other oxidation states of Hg and/or of other black amorphous material could not be excluded. Additionally, the low intensity of the metacinnabar XRD peaks might be both due to the nanometer scale of the superficial alteration and/or the dilution of the β-HgS peaks among α-HgS and/or an amorphous compound [22]. More recently, Oujja et al. have determined by XPS the change of phase of raw α-HgS into β-HgS upon irradiation at 1064 nm (laser pulses of 15 ns and 150 ps) and at 213 nm (laser pulses of 15 ns). Both lasers favored thermal heating of the studied area [23].

Béarat et al. [19] evaluated the influence of a Raman spectrometer laser and noted the decomposition of cinnabar and subsequent volatilization of mercury and sulfur, with no transformation into metacinnabar. Interestingly, they associated a number of distinctive Raman scattering peaks to natural polycrystalline metacinnabar, while β-HgS has been established as a poor Raman scatterer by other scholars [14] or found to have an identical Raman spectrum to that of cinnabar but with reduced intensity [11]. Similarly, Philippidis et al. [24] concluded that the predominant deterioration phenomenon of cinnabar caused by lasers used in Raman spectrometers is laser-induced heating that causes blackening and crater formation with material loss and Hg (either liquid or gaseous) and S (gaseous) release. The Raman intensity decreased by over an order of magnitude and no new spectral features were detected. According to the XRD results, α-HgS was identified both in intact and altered areas. However, the authors attributed the darkening to the formation of black metacinnabar, possibly below the limit of detection of the technique.

Yu et al. [16] have studied the damage induced by the femtosecond lasers of a pump-probe microscope at different illumination powers, which resulted into the conversion of α into β-HgS in areas that already contained grains of β-HgS, a detected impurity in red cinnabar. This conversion, which is thought to occur through an intermediate state, yet to be defined, is enhanced by higher temperatures, favored by local heating created by already existing β-HgS upon laser exposure (multiphoton-induced, temperature-sensitive photochemical reaction).

Although, as it has been introduced above, different scholars have evaluated the influence of lasers on the stability of cinnabar, to the authors' knowledge, the possible transformation products that can be formed by the influence of lasers implemented in instruments for laser-induced breakdown spectroscopy (LIBS) has not yet been investigated.

The main goal of this work is to evaluate whether Pompeian cinnabar used in fresco paintings (calcium carbonate as binder) experienced a transformation to metacinnabar due to the thermal impact caused by the 79 AD volcanic eruption of Mount Vesuvius and whether this last crystalline phase is stable at room temperature. The possible role of the pyroclasts deposited on the Pompeian frescoes in its stabilization at room temperature or even preventing the sublimation of the mercury was also studied. Moreover, the hypothetical additional stabilization of metacinnabar at room temperature by the action of metallic traces present in the original mineral cinnabar ores employed to prepare the Pompeian pigment was also explored, after an elemental characterization of original Pompeian cinnabar pigment, ground mineral ores and a synthetic pigment. For that, mineral specimens from the Almadén mining district have been considered, the main cinnabar source of the Roman period as it has been mentioned above. To achieve all the mentioned objectives, temperature-resolved X-ray diffraction (XRD) and XRD monitoring experiments have been conducted using powdered cinnabar mineral samples from the mentioned source and cinnabar-decorated mock-ups, respectively.

As cinnabar pigment is frequently studied using laser-based techniques, this work also aims to confirm if possible false positives in the detection of metacinnabar after the interaction of the lasers implemented in LIBS instruments with cinnabar pigment can be obtained. For that, darkened cinnabar residues promoted by the impact of a laser implemented in a portable LIBS system have been studied by XRD, X-ray photoelectron spectroscopy (XPS) and scanning electron microscopy coupled with energy-dispersive X-ray spectroscopy (SEM–EDS).

2 Materials and methods

2.1 Samples, mural paintings and fresco mock-ups

Pompeian fresco painting samples (fragments) and the mural paintings considered in this work belong to the House of Marcus Lucretius (Regio IX 3, 5/24) from the Archaeological Park of Pompeii (Italy). Concretely, among painting fragments, samples ATT2007/14 and 16/56 belong to the *triclinium* of the house and were extracted from mural paintings impacted by the 79 AD eruption of Mount Vesuvius. Additionally, samples protected from the eruption recovered from the same house were also considered (3T and Red A). For more information about the samples, see details elsewhere [5, 25, 26].

The red cinnabar pigment used to prepare the fresco mock-ups was purchased from Kremer Pigmente (Aichstetten, Germany). Cinnabar mineral specimens from the Almadén mining district (Almadén and Las Cuevas locations) were kindly provided by Minas de Almadén y Arrayanes S.A (MAYASA) (Castilla-La Mancha, Spain). Before the XRD experiments and the SEM–EDS analyses, mineral specimens were manually ground in an agate mortar. A cinnabar pigment recovered from the archaeological excavations of Pompeii was also analyzed by SEM–EDS and compared with the synthetic pigment (Kremer Pigmente), but it was not employed for the thermodiffractometry studies due to the low quantity of material available and the destructive nature of the measurements.

Biocalce Pietra and Biocalce Intonachino Fino (Kerakoll, Castellón de la Plana, Spain) were used to prepare the fresco mock-ups. Biocalce Pietra, composed by natural hydraulic lime, natural pozzolana, fluvial silica sand and dolomitic limestone, was left to set as the *arriccio* (inner mortar, prepared by mixing 30 g of the mentioned mortar and 5.4 mL of deionized water for each mock-up), whereas Biocalce Intonachino Fino, composed by natural hydraulic lime, fluvial silica sand and pure marble powder, was extended as the *intonaco* (outer mortar, prepared by mixing 3 g of the mentioned mortar and 0.9 mL of deionized water for each mock-up) and painted with a suspension of cinnabar pigment in Milli-Q water, while the *intonaco* was still fresh. The final thickness of the *arriccio* was 1.5 cm and that of the *intonaco* 200 μm. The *arriccio* was left to cure during 24 h before applying the intonaco. Once each mock-up was painted, the *intonaco* was allowed to set for 24 h before subjecting the mock-ups to any analysis or aging experiment.

To paint the mock-ups, a commercial cinnabar pigment (7 mock-ups) and powdered mineral from Las Cuevas (7 mock-ups) were used, respectively. For their application as pigment, the mineral specimens were manually ground in an agate mortar.

2.2 Instrumentation

Three portable instruments were considered in this work. An Innov-X Alpha Series (Innov-X Systems Inc., Woburn, MA, USA) handheld energy-dispersive X-ray fluorescence spectrometer (HH-EDXRF), which implements an Ag-anode X-ray tube, was used. Measurements were acquired at 35 kV and 5 mA during 60 s. Moreover, a portable innoRam Raman spectrometer (B$_\&$WTEK$_{INC.}$, Newark, NJ, USA) was also considered. For more information about these two portable instruments see elsewhere [5, 27]. Lastly, a Nd:YAG laser implemented in a portable LIBS device (EasyLIBS IVEA, model Easy 2C) which operates in a dual-pulse mode, emitting at a wavelength of 1064 nm, was also employed. The laser energy per pulse on the surface was lower than 25 mJ at 1 Hz.

Three different diffractometers were used in this study. First of all, a X'PERT PRO automatic diffractometer (PANalytical, Almelo, Netherlands) was employed. The operating conditions were 40 kV and 40 mA, in theta-theta configuration, secondary monochromator with Cu Kα radiation (λ = 1.5418 Å) and a PIXel solid-state detector.

The XRD D8 Advance diffractometer, which operates at 30 kV and 20 mA and is equipped with a Cu tube (λ = 1.5418 Å), a Vantec-1 PSD detector and an Anton Parr HTK2000 high-temperature furnace, was also used. The powder patterns were recorded in 2θ steps of 0.033º for different 2θ ranges and heating/cooling rates, using a Pt sample holder.

Finally, the last diffractometer considered was the D8 Discover diffractometer (Bruker AXS Advanced X-ray Solution GmbH, Karlsruhe, Germany), equipped with a Cu Twist tube, Ni filter (λ = 1.5418 Å), PolyCap^{TM} (1-μm single-crystal cylinders) system for parallel beam generation (divergence of 0.25°) and a 1-D LynxEye detector (active length in 2θ 2.7º). The samples were mounted on an Eulerian Cradle with automatic controlled XYZ stage.

For all the XRD measurements, the mineral phase identification was performed using the X´pert HighScore software, by comparing the obtained diffractograms with the list of standards included in the Powder Diffraction File-4 2021 (ICDD) database.

As it will be explained in the next section, a JEOL JSM-7000-F (JEOL, Tokyo, Japan) SEM–EDS (Oxford instruments INCA, Energy 350, Oxfordshire, UK) was also implemented in the analytical methodology. To improve the conductivity of the samples for the image acquisition, they were coated by depositing $\approx$ 20 μm of a carbon layer. For additional technical details, please see elsewhere [5].

Lastly, the XPS instrument (SPECS System, Berlin, Germany) implemented in the analytical strategy is equipped with a Phoibos analyzer 150 1D-DLD and monochromatic Al Kα (1486.7 eV) X-ray source.

2.3 Analytical methodology

Table 1 presents a summary of the portable and laboratory instrumentation used to analyze the samples (Pompeian fresco paintings and pigment), mural paintings and fresco mock-ups considered in this work.

Table 1 Laboratory and portable instrumentation used in this study to analyze the samples (Pompeian fresco paintings and cinnabar pigments), mural paintings and fresco mock-ups

Samples and paintings	HH-EDXRF	Portable Raman	Portable LIBS	XRD	SEM–EDS	XPS	Raman microscopy
Pompeian painting samples				×	[5]		[5]
HML mural paintings	×	×					
Mock-ups (CP)			×	×	×	×	
Mock-ups (CP and LC coated with pyroclasts)				×			
Pompeian pigment					×		
Commercial pigment			×		×		
Powdered samples from ALM and LC				×	×		

Painting samples: ATT2007/14, 16/56, 3T, Red A
HML House of Marcus Lucretius; *CP* Commercial Pigment; *LC* Las Cuevas mineral; *ALM* Almadén mineral

To confirm/reject the formation of metacinnabar in the Pompeian fresco painting samples exposed and non-exposed to the 79 AD volcanic event, the X'PERT PRO automatic diffractometer was used. All the fragments were analyzed without any sample preparation. In addition, the wall painting from which sample ATT2007/14 and 16/56 were extracted was in situ analyzed by portable Raman spectroscopy.

To faithfully simulate the real impact of the pyroclastic flow into the wall painting, the cinnabar fresco mock-ups were thermally exposed in an external Nabertherm GmbH Model LT9/12/B180 furnace at different temperatures (30, 100, 250, 280, 310, 340, 370 °C) using a 10 °C/min heating rate. After the end of the cycle, the mock-ups were kept in the muffle, while it cooled down at a speed of 1 °C/min. The X-ray powder diffraction patterns were collected directly by using a X'PERT PRO automatic diffractometer (PANalytical, Almelo, Netherlands).

Experimental results obtained in the laboratory by analyzing the mock-ups were complemented with in situ Hg detection in Pompeian mural paintings of the House of Marcus Lucretius employing the HH-EDXRF spectrometer.

Powdered cinnabar mineral samples from the Almadén mining district sealed into glass capillary and a cinnabar fresco mock-up were subjected to temperature-resolved XRD experiments using the D8 Advance diffractometer. A powdered mineral sample from Almadén was sealed into a glass capillary tube and heated from 30 to 400 °C (10 °C increment every 12 min) and cooled from 400 to 30 °C. The cinnabar mineral powder from Las Cuevas was also thermally exposed. In this case, the sample was also subjected to the same increments of temperature from 30 to 300 °C, but from 300 to 400 °C, diffractograms were acquired every 2 °C.

To evaluate the transformation of the cinnabar due to the impact of a laser implemented in a LIBS spectrometer, the laser pulses coming from a pulsed Nd:YAG laser implemented in the mentioned portable LIBS device were applied by directly placing the sampling interface on a cinnabar fresco mock-up, painted with commercial pigment, and on a pressed pellet of commercial pigment. X-ray powder microdiffraction patterns of the black deposits formed after the impact of the laser were collected directly using the D8 Discover diffractometer. The formed LIBS microcraters were also morphologically and chemically analyzed by means of SEM–EDS and XPS.

3 Results and discussion

3.1 Characterization of cinnabar-decorated Pompeian wall paintings and temperature-resolved XRD experiments

Cinnabar-decorated painting fragments (ATT2007/14 and 16/56, 3T and Red A samples) extracted from mural paintings of Pompeii were previously analyzed using SEM–EDS and Raman microscopy, being possible to identify calomel in samples ATT2007/14 and 16/56, exposed to the volcanic eruption, but not in the protected ones (3T and Red A) [5]. The additional XRD analyses performed in the context of this work on all these fragments did not confirm the presence of metacinnabar, neither on the samples protected from the volcanic eruption nor on those affected by the thermal impact. See the diffractograms of 16/56, a sample exposed to the 79 AD volcanic eruption, and Red A, not exposed, in Fig. S1a. As cinnabar is randomly present in mixture with ochre pigment [5], its detection in sample 16/56 by XRD is challenging. Figure S1b presents a Raman spectrum, acquired on the wall from which sample 16/56 was taken, showing the characteristic Raman bands of cinnabar (143, 254, 284 and 343 cm^{-1}).

In the cinnabar fresco mock-up painted using the synthetic pigment and subjected to the temperature-resolved XRD experiments (from 30 to 370 °C, including the cooling down), an amorphous-black color was observed (see Fig. S2), although no differences could be recorded in the diffractograms. Radepont et al. [4] reported an intermediate dark brown state of red mercury sulfide during heating which did not correspond to crystalline metacinnabar. After the thermal experiment conducted in this work, only cinnabar and calcite peaks were detected in the diffractograms. However, the intensities of the diffraction peaks of cinnabar in correlation

Table 2 Cinnabar to calcite ratios calculated for two different cinnabar diffraction peaks (26.20 and 30.94 2θ) during the exposure of a cinnabar fresco mock-up to a thermal cycle, starting at 30 °C with ramp up to 370 °C, maintaining that temperature for 1 min and cooling back to 30 °C

Temperature (°C)	α-HgS (26.20 2θ)/CaCO$_3$ (29.44 2θ)	α-HgS (30.94 2θ)/ CaCO$_3$ (29.44 2θ)
30	1.314	1.4628
370	0.23022	0.19237
370 (after 1 min)*	0.12468	0.10296
30 (cooling)	0.11261	0.08852

*3-min fast scan in this case

Fig. 1 Blackened cinnabar painting fragments consolidated on the southern wall of the *exedra* G of the House of the Golden Cupids and detail of the area of interest

with the ones of calcite were lower at the end of the thermal experiment. This, together with the appearance of the mock-up after the thermal cycle (see the absence of cinnabar layer at the end of the experiment in Fig. S2), suggests that the mercury was sublimated during the thermal exposure at temperatures not higher than 370 °C (see Table 2).

The sublimation of mercury from isolated cinnabar in powder state was also reported in previous thermal experiments [4]. This work proves that the binding ability of calcium carbonate to fix the cinnabar pigment to the wall is not enough to prevent its sublimation.

In some areas of the blackened cinnabar-decorated southern wall of Room G of the House of the Golden Cupids in the Archaeological Park of Pompeii, the underlying *intonaco* is visible and the original cinnabar pictorial layer seems to be absent (fading of the pigment). Thus, it is possible to observe gaps in the painting layer (see Fig. 1).

This is not the unique example of a cinnabar-decorated area that could have lost cinnabar mass through mercury sublimation as a consequence of the thermal impact promoted by the 79 AD volcanic eruption. An additional example could be the *tablinum* of the House of Marcus Lucretius. In the painting of its north wall, mercury traces were detected by HH-EDXRF (ranging from 1066 to 3360 mg/kg according to the semi-quantitative estimation), although the color of the walls has faded (see Fig. S3). The relevance of this room, in which the *dominus* received his guests, suggests the use of an expensive pigment —not visually observable nowadays— on the walls to show the wealthy position of the family.

Moreover, a visual inspection of the *triclinium* of this last house suggests a similar scenario. In this room, a mixture of hematite and cinnabar was used in the frames of the figurative panels and the architectural decoration [5]. As it can be observed in Fig. S4, the high temperatures of the pyroclastic density currents induced the transformation of yellow into red ochre on the right area of the north wall [28, 29], while the utmost left area was preserved. Interestingly, the left red frame remains intact, while the right red frame has lost pigment mass, most probably associated with the mercury sublimation coming from the use of red cinnabar applied in the mixture.

To explore if the pyroclastic materials deposited on the mural paintings of Pompeii in the 79 AD could have precluded the complete mercury sublimation, further experiments were performed. Different mock-up fragments were prepared and covered with the mixture of pyroclastic materials in order to expose them to different temperatures (30, 100, 250, 280, 310, 340, 370 °C) in a furnace. In order to compact the pyroclasts on the decorated surface, the later were mixed with the calcareous mortar Biocalce Pietra used to prepare the mock-ups.

After the exposure to each specific temperature, the coating of pyroclasts and calcareous mortar was removed from each mock-up fragment and XRD measurements were taken on the decorated surface. As can be observed in Fig. 2, at high temperatures the cinnabar paint layer disappeared. The visual observation at the microscale (see Fig. S5) indicated that the pyroclastic coating was not enough to avoid the sublimation of mercury at temperatures higher than 310 °C, when the painting layer starts to disappear (see Fig. 2). Even if the fragments painted using Las Cuevas cinnabar mineral were partially blackish, metacinnabar was not detected in this case. This last could suggest that, during the thermal impact, metacinnabar was not formed, since mercury sublimates at a temperature lower than the necessary one for the phase transition. However, its concentration in the paint layer could also be lower than the limit of detection of the technique (close to 5%).

Fig. 2 Cinnabar fresco mock-ups covered with a mixture of pyroclastic materials and calcareous mortar to simulate a closed system: **a** painted with the commercial pigment, **b** painted with the mineral from Las Cuevas, **c** appearance of the fresco mock-ups after the thermal aging at different temperatures and the subsequent removal of the deposited pyroclastic layer (commercial pigment on the left and Las Cuevas mineral on the right side)
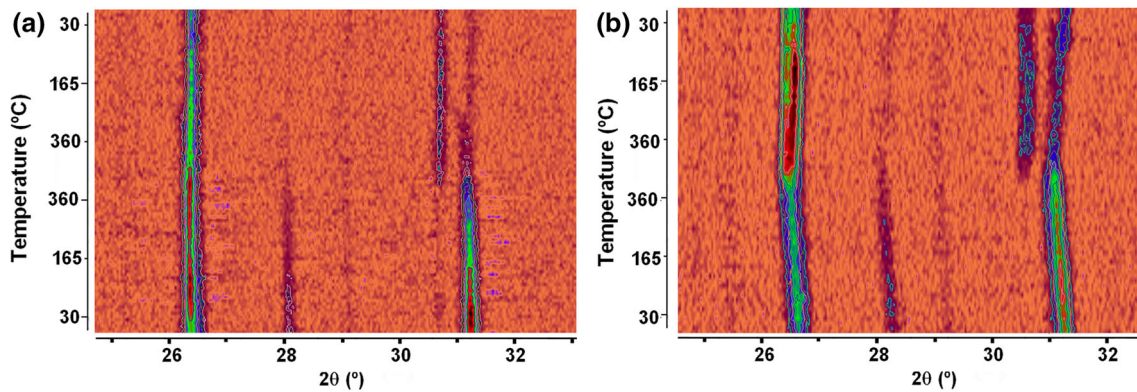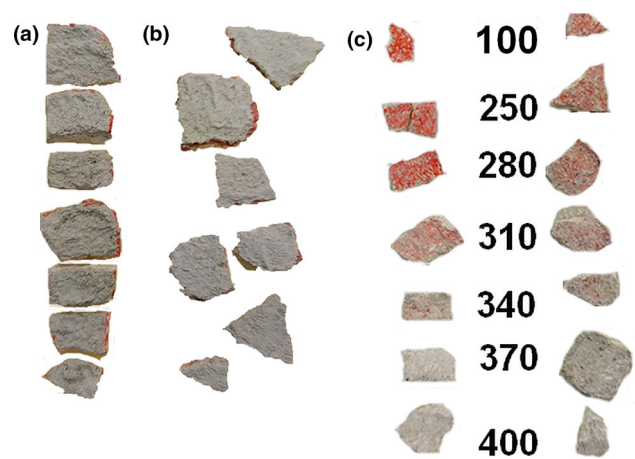
Fig. 3 Background-corrected thermodiffractometry intensity maps of the cinnabar ores encapsulated in capillary tubes: **a** Almadén and **b** Las Cuevas. The diffraction peaks of cinnabar (26.29, 27.93 and 30.94 2θ), calcite (29.44 2θ) and metacinnabar (26.43, 30.61 2θ) are visible, and their intensity varies depending on the step of the thermal cycle

Figure S6 presents the EDS spectra of a cinnabar pigment recovered in Pompeii, ground mineral from Almadén and Las Cuevas and commercial pigment from Kremer Pigmente. While the Pompeian pigment and the ground ores show metallic impurities, mainly Fe and Ti, the synthetic pigment is substantially more refined.

As some authors reported that metallic impurities (e.g., FeS_2, ZnS) not correctly removed from the cinnabar mineral could have an influence in the transformation process of the final pigment prepared [6], additional thermal experiments were conducted using ground cinnabar minerals from the Almadén mining district, to evaluate the effect of the thermal impact without the contribution of the mortar matrix. Since the quantity of available Pompeian pigment is limited, further experiments were performed only with the mineral ores.

When a powdered mineral sample from Almadén, sealed into a glass capillary tube, was heated, a characteristic diffraction peak of metacinnabar (30.61 2θ) was detected (see Fig. 3a) starting from 360 to 370 °C, apart from the 30.94 2θ peak of cinnabar observed since the beginning of the thermal cycle. Note how the 27.93 and 30.94 2θ peaks of cinnabar partially lost their intensity due to the conversion of cinnabar into metacinnabar, but not the 26.29 2θ peak of cinnabar, since it is superimposed with the 26.43 2θ metacinnabar peak.

The slower heating slope for the last temperature interval in the case of the cinnabar powdered ore of Las Cuevas, sealed in a glass capillary tube, and the maintenance of temperature at each high temperature for the acquisition of the diffractogram allowed the observation of the 30.61 2θ diffraction peak of metacinnabar starting from 330 °C (see Fig. 3b).

Metacinnabar was still present in the closed system upon slow cooling (see Fig. 4). The cinnabar diffraction peaks (26.29 and 30.94 2θ) and the metacinnabar peak (30.61 2θ) were present in all the spectra, although the relative proportion of the integrated areas changed throughout time. For example, the ratio of the integrated areas of the metacinnabar peak at 30.61 2θ versus the cinnabar one at 30.94 2θ was 1.05 right after the cooling, while it descended to 0.55 after 40 h.

3.2 Characterization of darkening of cinnabar induced by a laser implemented in LIBS instruments

The impact of the laser implemented in the portable LIBS system induced the formation of black residues on the crater generated on the surface of a cinnabar mock-up and a pressed pellet. In the case of the mock-ups, five laser pulses were enough to reach the inner

Fig. 4 a Powder diffractograms of Las Cuevas cinnabar mineral after thermal exposure (30–300–400–300 °C) and a slow cooling from 300 to 30 °C in 6 h (measurements performed right after the cooling, and 15 and 40 h later). **b** Las Cuevas cinnabar mineral powder before (top) and after the thermal exposure (bottom right), compared with intact cinnabar powder (bottom left)
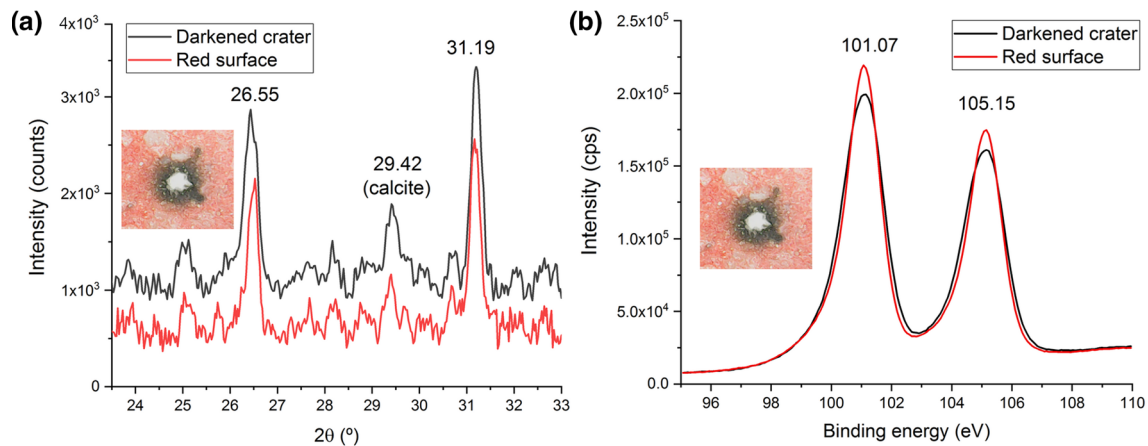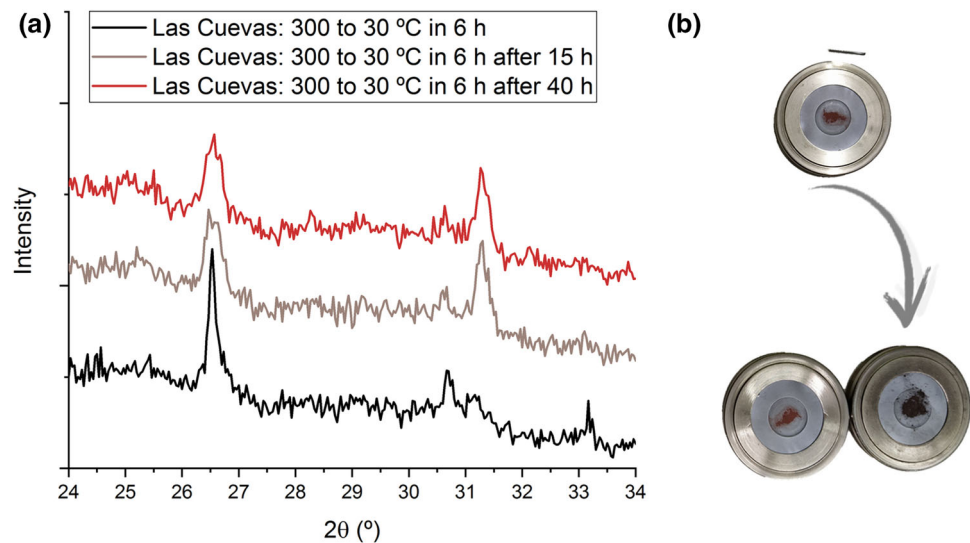
Fig. 5 a Microdiffractograms acquired on the darkened LIBS-induced crater and the intact red surface of a cinnabar fresco mock-up, **b** XPS spectra acquired on the darkened LIBS-induced crater and the intact red surface of a cinnabar fresco mock-up

mortar layer, as seen in Fig. 5. The black edge of the laser-induced crater was analyzed both by XRD and XPS. The diffractograms of the black area and the red intact surface were identical, without any peaks related to metacinnabar (see Fig. 5a). In addition, only Hg(2) was detected by XPS (see Fig. 5b) on both areas based on the two peaks at 101.07 and 105.15 eV (Hg 4f), corresponding to a spin–orbit splitting of 4.1 eV for the $4f_{7/2}$ and $4f_{5/2}$ states [30].

Afterward, the LIBS-induced crater formed on a cinnabar-pressed pellet was observed and analyzed by SEM–EDS using both the secondary and backscatter electron detection. In Fig. 6a and b, the crater, the shock wave and the background surface are distinguishable.

The mechanical damage induced by the laser can be observed in Fig. 6, where 6c corresponds to the crater and 6d to the intact surface. This mechanical damage could explain the darker appearance of the shock wave due to a loss of HgS, compared with the crater, in which HgS could have been redeposited after each laser pulse.

In-detail SEM micrographs of the interphases between the crater/shock wave and the shock wave/intact background are visible in Figs. 6e and f, respectively.

Considering the interference of Hg in the S detection by EDS, Quantmaps were obtained for both elements to obtain an accurate distribution of both in the mapped area. Hg and S (see Figs. 6a, g and h) do not reveal a preferential loss of neither Hg nor S in the crater, just a physical damage caused by the ablation of HgS. This last also suggests that an accumulation of metallic mercury is not occurring.

Fig. 6 Micrographs acquired on a LIBS-induced crater on a cinnabar-pressed pellet. **a** Crater, shock wave and intact surface (secondary electrons, SE). **b** Crater, shock wave and intact surface (backscattered electrons, BSE). **c** Detail of the crater (SE). **d** Detail of the intact surface (SE). **e** Interphase between the crater and the shock wave (SE). **f** Interphase between the shock wave and the intact surface (SE). **g** Hg Quantmap. **h** S Quantmap
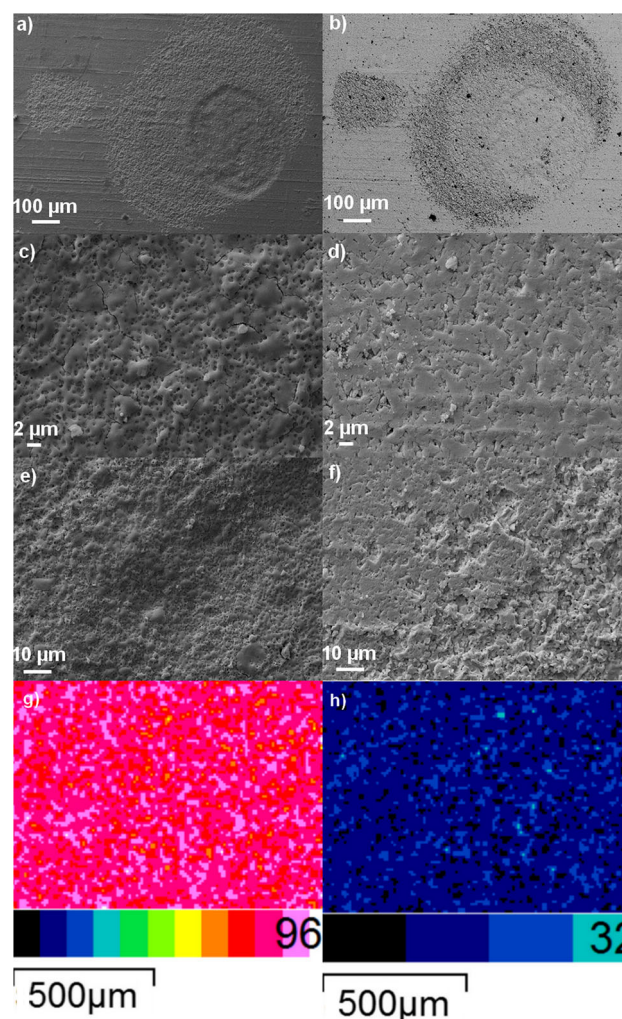
4 Conclusions

All the experimental evidence confirms that metacinnabar cannot be formed in a cinnabar-decorated fresco painting as a consequence of a thermal impact such as the one that took place in Pompeii due to the Mount Vesuvius eruption of 79 AD.

Thermodiffractometric experiments conducted using cinnabar-decorated fresco mock-ups proved that cinnabar became black (and amorphous), and afterward disappeared due to mercury sublimation before reaching the necessary temperature conditions to convert into crystalline metacinnabar. These experimental results agree with what is observable today in cinnabar-decorated Pompeian wall paintings: non-detection of metacinnabar and fading/losing of cinnabar pigment in some specific paintings. As pigment loss due to mercury sublimation is not observable in all cinnabar paintings of Pompeii, this could be also an indication of the irregular thermal impact of the Pyroclastic Density Currents of the 79 AD volcanic eruption on the wall paintings. This conclusion indicates that in-depth microscopic studies of specific mural paintings are needed to trace the possible original application of cinnabar decorations not visible nowadays to the naked eye.

On the contrary, in the thermal experiments conducted in this work, when cinnabar was exposed in a closed system, metacinnabar was detected. When the cooling was performed slowly, metacinnabar was still present at room temperature. This suggested that both a closed system and a slow cooling are necessary to ensure the stability of metacinnabar back at room temperature. However, this closed environment was not possible in the open-air mural paintings of Pompeii, even when the houses were under the non-compact pyroclastic materials, evidencing the lower possibilities to detect metacinnabar years after the eruption.

To confirm this hypothesis, the additional experiments simulating the possible sealing action of the pyroclastic materials when Pompeii was buried showed that, due to the porosity of the pyroclasts, expected according to their mineralogical composition, assessed in a previous publication [31], the cinnabar pigment was still able to sublimate and no metacinnabar was detected after the thermal aging. The same result was obtained even using not purified cinnabar directly extracted from the mineral ore of the Almadén mining district. Therefore, according to this last experiment, the impurities present in the mineral ore do not promote the stabilization of metacinnabar at room temperature in the kind of mock-ups prepared for this study. Thus, it can be concluded that,

even if metacinnabar could have been formed due to the thermal impact of the volcanic eruption of 79 AD, it would hardly be stable back at room temperature.

Although the thermal experiments here reported demonstrate that all or most of the cinnabar pigment mass from thermally aged mock-ups sublimates, in the future, it will be convenient to analyze high-temperature-impacted painting samples from Pompeii at micro/sub-micrometric scale (e.g., synchrotron-based experiments) to ensure that metacinnabar or metallic mercury micro-/nanoparticles have not been retained in the pictorial layer.

To finish, concerning the results here obtained, the impact of a LIBS Nd:YAG laser such as the one used in this work could only promote the amorphization of red cinnabar into a black species in the shock wave, being impossible to detect metacinnabar nor Hg(0). Hence, it can be affirmed that the thermal effect of this kind of laser does not induce the α-β crystalline phase transition.

Data Availability Statement The datasets generated during and/or analyzed during the current study are available from the corresponding author on reasonable request.

Declarations

Conflict of Interests The authors declare that they have no known competing financial interests or personal relationships that could have appeared to influence the work reported in this paper.

References

1. J. Trinquier, Rev. Archéologique **56**, 305 (2013)
2. J. Gwilt, *Translator, The Architecture of Marcus Vitruvius Pollio, In Ten Books* (Priestley and Weale, London, 1826)
3. J. Bostock, H.T. Riley, *Translators, The Natural History of Pliny* (H. G. Bohn, London, 1855)
4. Radepont M., Understanding of chemical reactions involved in pigment discoloration, in particular in Mercury Sulfide (HgS) Blackening, PhD Thesis, Paris 6, (2013)
5. S. Pérez-Diez, A. Pitarch Martí, A. Giakoumaki, N. Prieto-Taboada, S. De Fdez-Ortiz Vallejuelo, A. Martellone, B. De Nigris, M. Osanna, J.M. Madariaga, M. Maguregui, Anal. Chem. **93**, 15870 (2021)
6. F.W. Dickson, G. Tunnel, Am. Mineral. **44**, 471 (1959)
7. R.W. Potter, H.L. Barnes, Am. Mineral. **63**, 1143 (1978)
8. R.L. Feller, Rep. Stud. Hist. Art **1**, 99 (1967)
9. S. Liberti, Boll. Dell Ist. Cent. Restauro **3–4**, 45 (1950)
10. J.K. McCormack, Miner. Deposita **35**, 796 (2000)
11. M. Spring, R. Grout, Natl. Gallery Tech. Bull. **23**, 50 (2002)
12. M. Cotte, J. Susini, N. Metrich, A. Moscato, C. Gratziu, A. Bertagnini, M. Pagano, Anal. Chem. **78**, 7484 (2006)
13. K. Elert, M. Pérez Mendoza, C. Cardell, Commun Chem. **4**(1), 1 (2021)
14. P. Vandenabeele, K. Lambert, S. Matthys, W. Schudel, A. Bergmans, L. Moens, Anal. Bioanal. Chem. **383**, 707 (2005)

15. I. Istudor, A. Dina, G. Rosu, D. Seclaman, G. Niculescu, E Conservation **2**, 24 (2007)

16. J. Yu, W.S. Warren, M.C. Fischer, Sci. Adv. **5**, 3136 (2019)

17. P. Ballirano, M. Botticelli, A. Maras, Eur. J. Mineral. **25**, 957 (2013)

18. R. Cioni, L. Gurioli, R. Lanza, E. Zanella, J. Geophys. Res. Solid Earth **109**, B2 (2004)

19. Béarat H., Chizmeshya A., Sharma R., Barbet A., and Fuchs, in *3rd Int. Conf. Technol. Sci. Archaeol. Conserv.* (Zarqa (Jordan), 2004)

20. P. Pouli, D.C. Emmony, C.E. Madden, I. Sutherland, Appl. Surf. Sci. **173**, 252 (2001)

21. V. Zafiropulos, T. Stratoudaki, A. Manousaki, K. Melesanaki, G. Orial, Surf. Eng. **17**, 249 (2001)

22. V. Zafiropulos, C. Balas, A. Manousaki, Y. Marakis, P. Maravelaki-Kalaitzaki, K. Melesanaki, P. Pouli, T. Stratoudaki, S. Klein, J. Hildenhagen, K. Dickmann, B.S. Luk'Yanchuk, C. Mujat, A. Dogariu, J. Cult. Herit. **4**, 249 (2003)

23. M. Oujja, M. Sanz, E. Rebollar, J.F. Marco, C. Domingo, P. Pouli, S. Kogou, C. Fotakis, M. Castillejo, Spectrochim Acta - Part Mol. Biomol. Spectrosc. **102**, 7 (2013)

24. A. Philippidis, A. Mikallou, D. Anglos, Eur. Phys. J. Plus **136**, 1194 (2021)

25. M. Maguregui, U. Knuutinen, K. Castro, J.M. Madariaga, J. Raman Spectrosc. **41**, 1400 (2010)

26. M. Maguregui, U. Knuutinen, I. Martínez-Arkarazo, A. Giakoumaki, K. Castro, J.M. Madariaga, J. Raman Spectrosc. **43**, 1747 (2012)

27. J.M. Madariaga, M. Maguregui, K. Castro, U. Knuutinen, I. Martínez-Arkarazo, Appl. Spectrosc. **70**, 137 (2016)

28. I. Marcaida, M. Maguregui, S. Fdez-Ortiz de Vallejuelo, H. Morillas, N. Prieto-Taboada, M. Veneranda, K. Castro, J.M. Madariaga, Anal. Bioanal. Chem. **409**, 3853 (2017)

29. I. Marcaida, M. Maguregui, H. Morillas, S. Pérez-Diez, J.M. Madariaga, Anal. Bioanal. Chem. **411**, 7585 (2019)

30. A.S. Kumar, S.J. Jiang, W.L. Tseng, J. Environ Chem. Eng. **4**, 2052 (2016)

31. S. Pérez-Diez, L.J. Fernández-Menéndez, H. Morillas, A. Martellone, B.D. Nigris, M. Osanna, N. Bordel, F. Caruso, J.M. Madariaga, M. Maguregui, Angew. Chem. Int. Ed. **60**, 3028 (2021)